

**A fibre forming smectic twist-bent liquid crystalline phase**

Journal:	<i>RSC Advances</i>
Manuscript ID:	RA-COM-11-2014-014669.R1
Article Type:	Communication
Date Submitted by the Author:	19-Dec-2014
Complete List of Authors:	Tamba, Maria; Otto von Guericke University, ANP Salili, Seyyed; Kent State University, Chemical Physics Zhang, Cuiyu; Kent State University, Liquid Crystal Institute Jakli, Antal; Kent State University, Chemical Physics; Mehl, Georg; University of Hull, Department of Chemistry Stannarius, Ralf; Otto-von-Guericke University Magdeburg, Institute of Experimental Physics Eremin, Alexey; Otto-von-Guericke University Magdeburg, Institute of Experimental Physics

**Article type: Communication**

**A fibre forming smectic twist-bent liquid crystalline phase**

*M.- G. Tamba<sup>ac</sup>, S.M. Salili<sup>b</sup>, C. Zhang<sup>b</sup>, A. Jákl<sup>b</sup>, G. H. Mehl<sup>c\*</sup>, R. Stannarius<sup>a</sup> and A. Eremin<sup>a\*</sup>*

M.-G. Tamba, R. Stannarius, A. Eremin, Department of Nonlinear Phenomena, Institute for Experimental Physics, Otto von Guericke University Magdeburg, Magdeburg, Germany

E-mail: alexey.eremin@ovgu.de

S. M. Salili, C. Zhang, A. Jákl

Liquid Crystal Institute, Kent State University, P.O. Box 5190, Kent, Ohio 44242-0001, USA

M- G. Tamba , G. H Mehl

Department of Chemistry, University of Hull, Hull HU6 7RX, UK

Keywords: complex fluids, fibres, optical materials, liquid crystals

**We demonstrate the nanostructure and filament formation of a novel liquid crystal phase of a dimeric mesogen below the twist-bend nematic phase. The new fibre-forming phase is distinguished by a short-correlated smectic order combined with an additional nanoscale periodicity that is not associated with density modulation.**

Understanding and controlling the dimensionality of properties of fluidic systems is crucial for a wide range of disciplines. Most fluids we know exhibit flow properties in all three spatial dimensions. Although fluid behaviour may occur in systems with reduced dimensionality too. Membranes are examples of two-dimensional fluids, which are important building blocks of living organisms. Fibres or filaments with cylinder-shaped free boundary represent one-dimensional (1D) structures. Fibre forming materials find a wide range of applications such as textile, composite materials and fibre optics. Full understanding of such materials is associated with clear scientific and technological implications, in particular, in the field of microfluidics.

Liquid crystals with molecules organized either in molecular layers or columns with orientational and positional order exhibit fluid-like order at reduced dimensionality. Such materials are characterized by structural correlation lengths  $\xi > 150$  nm, typically in the micrometer range<sup>1</sup>. A fundamental theoretical and experimental challenge is to find 2D and 1D fluid structures that can be confined to a fluid in a cylinder without walls. In case of Newtonian liquids, the Rayleigh-Plateau (RP) instability leads to breaking of a fluid cylinder into droplets, when the length-to-diameter ratio is larger than  $\pi$ <sup>2</sup>. Therefore, fibres typically rupture when they are longer than a critical length<sup>3</sup>. Nematic or cholesteric liquid crystals do not form stable cylinders with an aspect ratio larger than  $\pi$ . However, several types of smectic or columnar liquid crystals have been demonstrated to form freely-suspended filaments with very large slenderness ratios.<sup>4-6</sup> It appears that in these materials, a 2D transversal order is essential to achieve mechanical stability of the fibre structure. Materials with predominately nematic order are prone to the RP instability.

Recently, certain dimeric molecules were found to form a different type nematic phase below the typical nematic. This *pseudo-layered* twist-bend nematic phase ( $N_{tb}$ ), predicted by Dozov and Memmer, has added impetus to the search for 1D fluids<sup>7-19</sup>.

Although the  $N_{tb}$  phase might favour fibre formation due to its pseudo layering, none of the materials we tested formed freely suspended fibres. The only exception is a dimeric material in a novel so far unknown X-phase that appears below the  $N_{tb}$  phase. In this phase, the material forms very stable fibres, although their structure is very different from that of known smectics<sup>20,21</sup>.

In this paper, we report polarizing optical microscopy (POM), small-angle X-ray scattering (SAXS), freeze fracture transmission electron microscopy (FF-TEM) and scanning electron microscopy (SEM) studies and propose that the X - phase has a twist-bend smectic ( $Sm_{tb}$ ) structure with correlation lengths less than 12 nm, an order of magnitude smaller than any other currently known smectic system.

The investigated compound (Fig. 1) is characterized by a relatively short hydrocarbon spacer consisting of seven methylene units and two terphenyl units with lateral fluoro groups that induce a negative dielectric anisotropy; the synthesis and the experimental techniques are outlined in the ESI. The compound exhibits the following phase sequence on cooling: Isotropic 156.8°C N [1.03] 127.8°C N<sub>tb</sub> [0.38] (96.6°C X [3.51]) 77.4 °C Crystal, where N and N<sub>tb</sub> are conventional uniaxial and a twist-bend nematic phases, respectively. The values in square bracket are the transitions enthalpies [ $\Delta H$  in Jg<sup>-1</sup>]. In the monotropic X phase, the material forms freely-suspended filaments, as discussed later. We note here, that the reported compound is, at least to best of our knowledge, the first, which exhibits another liquid crystal phase below the N<sub>tb</sub> phase.

X-ray measurements of the magnetically-aligned samples show a pattern of the nematic phase with only orientational order (Fig. 2a). At 140 °C two small angle peaks with very low intensities at 1.9 nm and 3.9 nm were detected. The macroscopic order is reduced upon the transition into the twist-bend N<sub>tb</sub> phase (Fig. 2b), - the wide-angle diffraction arcs are broader, but no change in the character of the diffraction pattern could be detected. The small angle intensities occur at values of 12.0 nm and 3.9 nm at 110°C. It is also remarkable that the molecular alignment changes making a small angle to an external magnetic field. Wide-angle reflections indicate no positional order and a nematic character of the phase. On the transition into the X phase, measured at 90°C, the broad small-angle reflections turn into well-resolved peaks at right angles to the wide-angle maxima, correlating to 4.2 nm and 2.1 nm. The diffraction pattern would be consistent with a SmA phase, however this is not in line with optical polarizing microscopy studies, where features indicative of a tilted phase, such as schlieren texture, are observed. The correlation length estimated from the full width at half maximum (FWHM) is only about 11.7 nm (Fig. 2c, d), roughly three molecular lengths. It is much smaller than the micrometer-scale correlation length typical for most smectics. Hence, it is too small for a typical smectic phase (Fig. 2c, d). Interestingly,

such short smectic correlations have been found both in the nematic and optically-isotropic smectic phases of bent-core liquid crystals<sup>22,23</sup> and they were attributed to either smectic clusters in nematics or to frustrated layers in smectics. To decide if in our case we are dealing with smectic clusters in a nematic phase, or in a frustrated smectic phase, the nanoscale structure was additionally investigated using FFTEM technique. A typical texture is shown in Fig. 2(e). One can see in the same areas the simultaneous signatures of the twist-bend structure in form of fairly regular stripes with the periodicity of  $p = 10.5$  nm periodicity, and the step-like terraces characteristic of smectic layers. This suggests that the X phase can be interpreted as a twist-bend smectic ( $\text{Sm}_{\text{tb}}$ ) phase, in which the molecules not only form the heliconical axis, but also have a density modulated layered structure with a short-range correlation (Fig. 1f). Although such a structure is locally similar to the  $\text{SmC}^*$  phase of chiral molecules, it is also very different as here the pitch and the layer correlation lengths are orders of magnitude smaller than in  $\text{SmC}^*$ , and the molecules are non-chiral.

The optical properties of the material were investigated using polarising microscopy. On cooling from the isotropic phase on a bare glass substrate, the N phase appears with typical *Schlieren* texture. In cells with *polyimide treated* glass substrates, the nematic adopts a planar texture. Typical director fluctuations result in its flickering appearance. In cells with homeotropic anchoring condition in the N phase, the homeotropically aligned nematic texture transforms into a quasi-homeotropic texture with oily streaks in the  $\text{N}_{\text{tb}}$  phase. In case of planar anchoring, the  $\text{N}_{\text{tb}}$  phase with planar anchoring exhibits a ribbon texture where the ribbons often adopt a helical structure, as shown in Figs. 3 a and c. Spatially resolved optical birefringence measurements and detection of the optical slow axis were made by polarising light microscopy and a CRI Abrio Micro imaging system (Fig. 3b - d). The slow optical axis adopts a bend deformation with splay walls separating the regions of the director bent in the  $\text{N}_{\text{tb}}$  phase. The effective birefringence exhibits a modulation varying between 0.02 and 0.05 (Fig. 3b). On further cooling to the  $\text{Sm}_{\text{tb}}$  phase, the ribbon texture smoothens and becomes

disordered (Fig. 3d). In cells with bare glass substrates, flat ribbons develop (Fig. 3b). These ribbons have nearly uniform birefringence and the slow axis is aligned perpendicular to the growth direction. They are similar to the textures of planarly aligned smectics, which indicates a 1D modulation in the transverse direction.

Surprisingly, the structure of the X phase is capable of suppressing the RP instability and it favours the formation of LC filaments instead of planar films. Freely-suspended filaments consisting of fibre bundles were prepared by pulling an LC droplet suspended between two glass capillaries in the X phase (Fig. 4a, b). During pulling, a fluid bridge appears first. The shape of the bridge adopts a catenoid form at small length-to-diameter ratios. As the length increases, above a critical value, the bridge collapses into an ordered cylinder-shaped filament with two less ordered menisci (Fig. 4a). Over short time scales, the filament's diameter does not change during elongation. The LC material freely flows from the menisci into the filament, which indicates the fluid nature of the filament along its symmetry axis. Over longer time scales, a thinning occurs with the rate depending on temperature. Far in the X phase, the filaments are stable for several hours. Close to the X – N<sub>tb</sub> transition (<3K), the stability reduces to 1 – 2 minutes (Fig. 4c). The thinning process can be separated in three stages. The first stage is a fast collapse of an unstable bridge to the filament state (Fig. 4c). It is followed by a plateau of a slow and uniform thinning over an extended time interval. This stage can be interrupted by occasional rupture of single fibres and a stepwise decrease of the filament size. The final stage is a rapid collapse of the filament. At higher temperatures, the fibres become unstable. After the transition into the twist-bend phase N<sub>tb</sub>, once the length of the catenoid-shaped bridge exceeds the critical value, the neck of the bridge collapses without reaching a plateau.

The filaments appear optically birefringent (Fig. 4a, b). The optical slow axis is aligned perpendicular to the filament axis. The birefringence is estimated to be roughly  $0.04 \pm 0.01$  (the error is due to the uncertainty in determining the thickness of the filament). These

values are close to the birefringence of the textures in sandwich cells. The optical retardance profile across the filament exhibits several maxima (see inset in Fig. 4b). This suggests that thick filaments consist of several fibres, which is verified by scanning electron microscopy (SEM). For the SEM studies, the fibres were prepared in the  $Sm_{tb}$  phase and rapidly cooled to room temperature. The SEM picture shown in Fig. 5 shows that the filament consists of about 2  $\mu\text{m}$  thick fibrils. In contrast to smectic and columnar fibres of bent-core liquid crystals, the fibrils are entangled yielding an interwoven structure with uneven outer surface<sup>24</sup>.

In conclusion, we described the nanostructure of a novel phase characterized by a short-range smectic order and a pseudo layer twist-bend structure, which suggest a twist-bend smectic ( $Sm_{tb}$ ) phase structure. This phase appears below the fluid twist-bend nematic phase with no smectic order but with only a pseudo-layering. While previous examples of smectic and columnar fibres showed the requirement of two nanoscale periodicities (layering and modulation, or a 2-D lattice), here there is only pseudo-layering and a short-range smectic order. The microscopic structure of fibres is clearly different from those of the bent-core smectic and columnar liquid crystals. This represents a new type of fluid filament structure, and provides direction for the long-standing search of truly 1D fluids forming filaments. Although the exact mechanism of the fibre stability is yet to be clarified, a modulated structure of the phase or formation of smectic clusters may be responsible for the fibre forming behaviour.

### **Acknowledgements**

We acknowledge the financial support by the German Science Foundation (DFG, Project: ER/467-7), MGT and GHM acknowledge funding through the EU FP7 project BIND, the NMSF, Swansea for accurate mass spectra and the authors acknowledge the US National Science Foundation under grant DMR 1307674.

1. P. Oswald and P. Pieranski, *Taylor & Francis New York*, 2006.
2. L. Rayleigh, *Proc London Math Soc*, 1879, **10**, 4–13.
3. S. S. Bhattacharyya and Y. Galerne, *ChemPhysChem*, 2013, **15**, 1432–1446.
4. D. H. van Winkle and N. A. Clark, *Phys. Rev. Lett.*, 1982, **48**, 1407–1410.
5. A. Eremin, U. Kornek, S. Stern, R. Stannarius, F. Araoka, H. Takezoe, H. Nadasi, W. Weissflog, and A. Jákli, *Phys. Rev. Lett.*, 2012, **109**, 017801.
6. A. Jákli, D. Krüerke, and G. G. Nair, *Phys. Rev. E*, 2003, **67**, 051702.
7. V. P. Panov, R. Balachandran, M. Nagaraj, J. K. Vij, Tamba M G, A. Kohlmeier, and G. H. Mehl, *Appl. Phys. Lett.*, 2011, **99**, 261903.
8. M. Cestari, S. Diez-Berart, D. A. Dunmur, A. Ferrarini, M. R. de la Fuente, D. J. B. Jackson, D. O. Lopez, G. R. Luckhurst, M. A. Perez-Jubindo, R. M. Richardson, J. Salud, B. A. Timimi, and H. Zimmermann, *Phys. Rev. E*, 2011, **84**, 031704.
9. J. W. Emsley, P. Lesot, G. R. Luckhurst, A. Meddour, and D. Merlet, *Phys. Rev. E*, 2013, **87**, 040501.
10. J. W. Emsley, M. Lelli, A. Lesage, and G. R. Luckhurst, *J Phys Chem B*, 2013, **117**, 6547–6557.
11. L. Beguin, J. W. Emsley, M. Lelli, A. Lesage, G. R. Luckhurst, B. A. Timimi, and H. Zimmermann, *J Phys Chem B*, 2012, **116**, 7940–7951.
12. K. Adlem, M. Čopič, G. R. Luckhurst, A. Mertelj, O. Parri, R. M. Richardson, B. D. Snow, B. A. Timimi, R. P. Tuffin, and D. Wilkes, *Phys. Rev. E*, 2013, **88**, 022503.
13. V. Borshch, Y. K. Kim, J. Xiang, M. Gao, A. Jákli, V. P. Panov, J. K. Vij, C. T. Imrie, Tamba M G, G. H. Mehl, and Lavrentovich O D, *Nature Communications*, 2013, **4**.
14. V. P. Panov, R. Balachandran, J. K. Vij, Tamba M G, A. Kohlmeier, and G. H. Mehl, *Appl. Phys. Lett.*, 2012, **101**, 234106.
15. E. G. Virga, *Phys. Rev. E*, 2014, **89**, 052502.
16. P. K. Challa, S. N. Sprunt, A. Jákli, and J. T. Gleeson, *Phys. Rev. E*, 2014, **89**, 010501(R).
17. N. Vaupotic, M. Cepic, M. A. Osipov, and E. Gorecka, *Phys. Rev. E*, 2014, **89**, 030501.
18. J. Xiang, S. V. Shiyakovskii, C. T. Imrie, and O. D. Lavrentovich, *Phys. Rev. Lett.*, 2014, **112**, 217801.
19. E. Gorecka, M. Salamonczyk, A. Zep, D. Pocięcha, C. Welch, Z. Ahmed, and G. H. Mehl, *Liquid Crystals*, 2014 *accepted*
20. A. Nemeš, A. Eremin, R. Stannarius, M. Schulz, H. Nadasi, and W. Weissflog, *Phys. Chem. Chem. Phys.*, 2006, **8**, 469–476.
21. A. Eremin, A. Nemes, R. Stannarius, M. Schulz, H. Nadasi, and W. Weissflog, *Phys. Rev. E*, 2005, **71**, 031705.
22. A. Jákli, *Liquid Crystals Reviews*, 2013, **1**, 65–82.
23. W. Weissflog, S. Sokolowski, H. Dehne, B. Das, S. Grande, M. W. Schröder, A. Eremin, S. Diele, G. Pelzl Correspond, and H. Kresse, *Liquid Crystals*, 2004, **31**, 923–933.
24. C. Bailey, M. Murphy, A. Eremin, W. Weissflog, and A. Jákli, *Phys. Rev. E*, 2010, **81**, 031708.

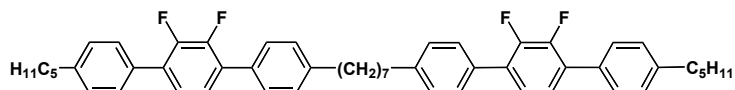


Fig. 1. Chemical structure of the investigated mesogen.

b)

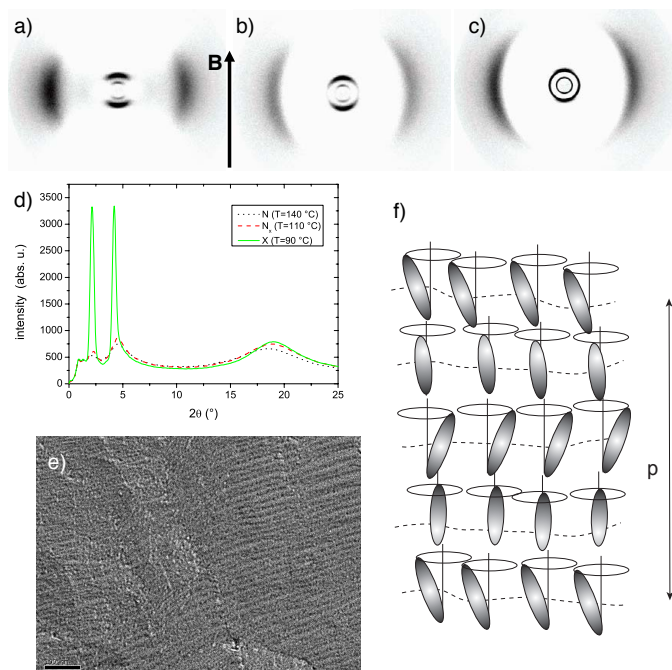
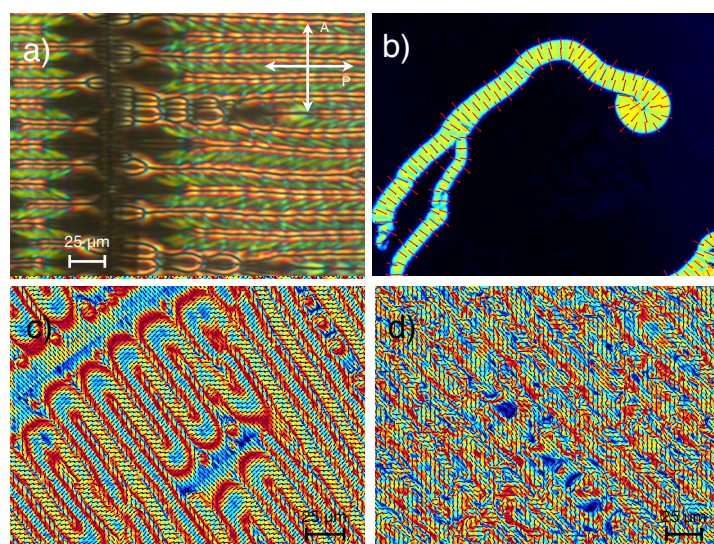
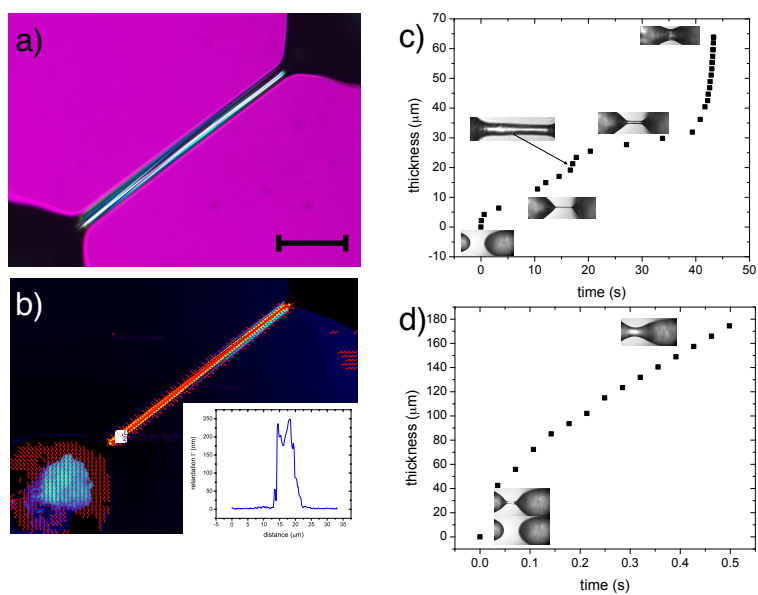


Fig. 2 X-ray patterns of magnetically ( $B=1T$ ) aligned samples in a) N phase  $T=140^{\circ}C$ , b)  $N_x$  phase ( $T=110^{\circ}C$ ), c) X phase ( $T=90^{\circ}C$ ), d) theta-scan of the powder samples; e) TEM images of the samples prepared in the X phase at  $T=90^{\circ}C$  (the scale bar corresponds to 100 nm); f) a schematic of a structure of the X phase showing smectic layers (dashed lines) and tilted mesogens forming a helical structure with a very short pitch  $p$ .



**Figure 3.** Polarising microscopy image of the  $N_x$  phase (a). Birefringence maps and the distribution of the slow axes visualised by Abrio Polscope (b-d): (d) a ribbon of the X phase growing on a glass substrate ( $T=93^{\circ}C$ ); c) A typical rope-texture in the  $N_{wb}$  phase transforms into a smooth disordered texture of the X phase in (d)



**Figure 4.** Freely suspended filaments: a) polarising microscopy image of a filament in the X phase ( $T=93^{\circ}\text{C}$ ) taken with a wave-plate; b) birefringence map of a filaments, the slow axis is aligned radially, the radial profile of the retardation is in the inset. Thinning dynamics of an LC bridge in the X c) and the  $N_x$  phases d).

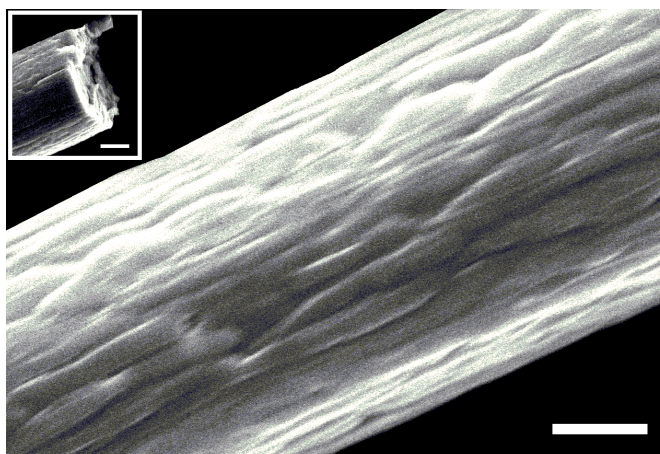


**Figure 5.** SEM micrograph of a fibre rapidly cooled in a highly viscous mesophase or a crystalline state. Individual fibrils are seen in the fibre as well as the fracture surface shown in the inset. The scale bars indicate 4 μm.